The Relationship between Precipitation and Precipitable Water in CMIP6 Simulations and Implications for Tropical Climatology and Change

SAMSON M. HAGOS,[a] L. RUBY LEUNG,[a] OLUWAYEMI A. GARUBA,[a] CHARLOTTE DEMOTT,[b] BRYCE HARROP,[a] JIAN LU,[a] AND MIN-SEOP AHN[c]

[a] *Pacific Northwest National Laboratory, Richland, Washington*
[b] *Colorado State University, Fort Collins, Colorado*
[c] *University of Washington, Seattle, Washington*

(Manuscript received 24 March 2020, in final form 25 November 2020)

ABSTRACT: It is well documented that over the tropical oceans, column-integrated precipitable water (pw) and precipitation (P) have a nonlinear relationship. In this study moisture budget analysis is used to examine this P–pw relationship in a normalized precipitable water framework. It is shown that the parameters of the nonlinear relationship depend on the vertical structure of moisture convergence. Specifically, the precipitable water values at which precipitation is balanced independently by evaporation versus by moisture convergence define a critical normalized precipitable water, pw_{nc}. This is a measure of convective inhibition that separates tropical precipitation into two regimes: a local evaporation-controlled regime with widespread drizzle and a precipitable water–controlled regime. Most of the 17 CMIP6 historical simulations examined here have higher pw_{nc} compared to ERA5, and more frequently they operate in the drizzle regime. When compared to observations, they overestimate precipitation over the high-evaporation oceanic regions off the equator, thereby producing a ''double ITCZ'' feature, while underestimating precipitation over the large tropical landmasses and over the climatologically moist oceanic regions near the equator. The responses to warming under the SSP585 scenario are also examined using the normalized precipitable water framework. It is shown that the critical normalized precipitable water value at which evaporation versus moisture convergence balance precipitation decreases as a result of the competing dynamic and thermodynamic responses to warming, resulting in an increase in drizzle and total precipitation. Statistically significant historical trends corresponding to the thermodynamic and dynamic changes are detected in ERA5 and in low-intensity drizzle precipitation in the PERSIANN precipitation dataset.

KEYWORDS: Climate change; Drizzle; Convective parameterization; Coupled models

1. Introduction

Understanding and quantifying the effects of global warming on regional hydrological cycles is one of the most important problems in climate science because of the societal implications. At global scale, atmospheric moisture increases with temperature under global warming at a rate that follows the Clausius–Clapeyron relationship of ~7% K^{-1}, while global precipitation increases at a much slower rate of ~2% K^{-1} (Held and Soden 2006). This difference between the responses of precipitation and atmospheric moisture content is related to the constraint imposed by the atmospheric radiative cooling due to the increased temperature and humidity, which limits the precipitation change through the global energy and water balances (Allen and Ingram 2002; Pendergrass and Hartmann 2014). Regional differences of the precipitation response are much less clear, particularly over the tropics, where spatial and temporal shifts related to dynamic and thermodynamic responses to warming can influence regional hydrology. This challenge is further exacerbated by the persistent precipitation distribution biases in generations of climate models, undermining our confidence in model projections of future changes in precipitation. The biases that are well documented in the simulations from phases 3 and 5 of the Coupled Model Intercomparison Project (CMIP3 and CMIP5, respectively) include excessive precipitation over oceanic regions off of the equator (Hirota and Takayabu 2013; Fiedler et al. 2020), weak South Asian monsoon rainfall (Hagos et al. 2019), and weak Amazon precipitation (Yin et al. 2013). Understanding the origin of these biases and how they relate to regional-scale projections of precipitation changes is critical for building confidence in the projections.

Several studies suggest that model precipitation biases are related to the representation of convection. For example, precipitation biases in coupled climate simulations can be reproduced in uncoupled Atmosphere Model Intercomparison Project (AMIP)-style simulations (Zhang et al. 2007; Chikira 2010) while some modifications to the parameterization of

Denotes content that is immediately available upon publication as open access.

Corresponding author: Samson Hagos, samson.hagos@pnnl.gov

DOI: 10.1175/JCLI-D-20-0211.1

convection, specifically the sensitivity of convection to environmental humidity, appear to mitigate the biases (Song and Zhang 2009; Hirota et al. 2011; Emori et al. 2001). The nonlinear relationship between convection and environmental humidity over the tropical oceans has been well documented (Bretherton et al. 2004; Rushley et al. 2018; Ahmed and Schumacher 2015, and references therein). Several studies empirically approximate the relationship using an exponential function with a ''pick-up'' precipitable water value at which precipitation starts to increase rapidly with precipitable water (Igel et al. 2017; Sahany et al. 2014). Conceptually this relationship provides a measure of the effectiveness of environmental air in diluting rising plumes in moist convection (Peters et al. 2009; Holloway and Neelin 2009, etc.) and the moistening effect of convection on the environment. Analyzing the nonlinear relationship between precipitation and precipitable water in the South Asian monsoon region and the equatorial Indian Ocean, Hagos et al. (2019) identified the normalized precipitable water in the equatorial Indian Ocean as an important metric for understanding model biases in simulating South Asian monsoon precipitation and the intermodel spread in future precipitation projections.

Extending the geographic focus from the South Asian monsoon region to the entire tropics, we aim to address two questions in this study: What are the origins of biases in CMIP6 precipitation climatology over the tropics? What are the implications of the biases for uncertainties in the projected changes? To this end, we first derive the precipitation–precipitable water relationship discussed above from the moisture budget equation and examine its representation in the historical and future climate simulations of the newest generation of models that participated in CMIP6 and in a global reanalysis. Then the relationship is normalized such that key parameters that control the model behavior in both historical and projection simulations are identified and their physical meanings in the context of model representation of convection are discussed.

2. Tropical precipitation climatology in CMIP6 simulations

We analyzed 17 historical simulations and 10 future simulations following the Shared Socioeconomics Pathway (SSP585) from the CMIP6 model archive. The models were selected based on availability of daily precipitation, precipitable water, and evaporation output, as required by the analysis. Where it is available vertically integrated moisture convergence is directly used; otherwise, it is estimated from the above listed variables using the moisture budget equation. We also analyzed data from the ERA5 dataset (C3S climate services 2017), two observational precipitation datasets, and an observational evaporation dataset. They are Precipitation Estimation from Remotely Sensed Information using Artificial Neural Networks (PERSIANN; Ashouri et al. 2015) and Tropical Rainfall Measuring Mission (TRMM 3B42; Huffman et al. 2010) and the Woods Hole Objectively Analyzed Flux Project daily evaporation data (OAFlux; Yu et al. 2008). All data are remapped to uniform 2° grid spacing. The study is focused on the tropics between 20°S and 20°N. We analyzed two 15-yr periods: 2000–14 for the historical simulations and 2086–2100 for the future simulations.

In Fig. 1, we compare the mean precipitation from the 17 CMIP6 models for the historical period to the mean observed precipitation, computed as the average of TRMM and PERSIANN precipitation. Compared to observations, the CMIP6 multimodel mean shows excessive precipitation over the tropical oceans off the equator and drier conditions over the tropical landmasses. Figure 2 shows the climatological mean of the daily low-intensity precipitation, or drizzle, and evaporation. For reasons that will be apparent in the next section, drizzle is defined as precipitation rates less than 0.13 mm h^{-1} (3.12 mm day^{-1}). The models have particularly excessive low-intensity precipitation, which has been well documented for previous generations of models (Sillmann et al. 2013; Liu et al. 2014; Stephens et al. 2010; Dai 2006). The corresponding evaporation fields are shown in the right column of Fig. 2. Excess evaporation is also a common bias in previous generation of models. In the tropics, this bias is driven primarily by wind biases (e.g., Small et al. 2019), but also possibly related to biases in downwelling shortwave radiation and model resolution (Demory et al. 2014). The spatial similarities between the biases in total precipitation (Fig. 1c), drizzle (Fig. 2c), and evaporation (Fig. 2f) are striking and will be discussed later.

The effects of tropical oceanic rainfall and 850-hPa wind biases on precipitable water over tropical landmasses are shown in Fig. 3. Excessive CMIP6 rainfall over the tropical oceans diverts moisture away from the tropical lands, weakening the moisture transport to South Asia, Africa, and the Amazon, resulting in dry biases over land regions. As the circulation biases may be induced by precipitation biases over the oceans through diabatic heating, we hypothesize that better representation of the climatology of precipitation over the oceans could reduce the perennial dry biases over land in generations of models (Sperber et al. 2013). This hypothesis will be examined in the next section.

3. The relationship between precipitation and precipitable water

a. Derivation

To investigate the origins of model precipitation biases, we first examine the processes behind the observed relationship between precipitation and precipitable water. Consider the vertically integrated moisture budget equation:

$$\frac{\partial(\mathrm{pw})}{\partial t} = E - P - \frac{1}{g}\int_{\mathrm{pt}}^{\mathrm{ps}} \nabla \cdot (\mathbf{v}q)\, dp, \tag{1}$$

where

$$\mathrm{pw} = \frac{1}{g}\int_{\mathrm{pt}}^{\mathrm{ps}} q\, dp \tag{2}$$

is the column-integrated water vapor or precipitable water; E and P are evaporation and precipitation respectively, while ps and pt are the pressures at the surface and top of the atmosphere, respectively. To obtain a relationship between precipitation and precipitable water, the moisture convergence

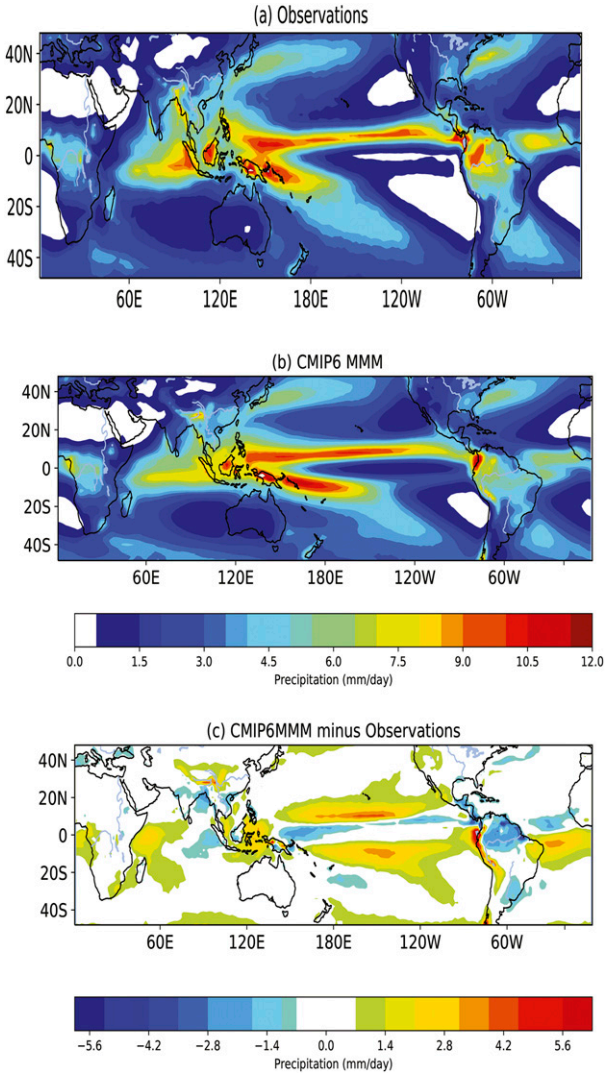

FIG. 1. 15-yr (2000–14) mean precipitation from (a) TRMM-3B42 and PERSIANN (mm day^{-1}) and (b) multimodel mean of the 17 CMIP6 historical simulations, and (c) the difference of (b) minus (a).

term has to be represented as a separable function of P and pw. To do that we introduce a variable, normalized moisture flux convergence (NMFC), as

$$\text{NMFC} = \frac{-\frac{1}{g}\int_{\text{pt}}^{\text{ps}} \nabla \cdot (\mathbf{v}q)\, dp}{\text{pw}} \tag{3}$$

such that the moisture budget equation can be written as

$$\frac{\partial(\text{pw})}{\partial t} = E - P + (\text{NMFC})\text{pw}. \tag{4}$$

As can be seen from its definition, NMFC is related to the vertical structure of wind divergence in relation to moisture profile. Therefore, by continuity it is related to vertical velocity. Over the tropical oceans tropospheric temperature gradients are weak and diabatic heating is primarily balanced by adiabatic cooling (Sobel and Bretherton 2000; Sobel et al. 2001), leading to a relationship among vertical velocity, static stability, and diabatic heating (see the appendix). Using conservation of moisture, mass, and energy, the relationship between moisture flux convergence and precipitation was obtained in Hagos et al. (2019). Here we focus the discussion on the physical interpretations and implications for subsequent analysis. As is apparent from (4), NMFC plays an important role in moisture variability so its physical interpretation deserves some discussion. Figure 4a shows the relationship between wind divergence (contours) and moisture normalized by the column integrated precipitable water [i.e., $(q/\text{pw})(dp/g)$; shading] over the tropical oceans between 20°S and 20°N based on ERA5. For precipitation less than about 0.13 mm h^{-1}, there are strong upper-level convergence and near-surface divergence indicating subsidence and convective inhibition. For precipitation greater than about 0.13 mm h^{-1}, near-surface convergence (dashed green contours) increases and deepens, and the height of maximum divergence (Fig. 4a, red contours) increases. The profile of water vapor mixing ratio (i.e., the moisture mixing ratio normalized by precipitable water) is displayed in shadings. This profile shows little change with increasing precipitation. Increases in the height level of maximum divergence as well as an increase in low-level moisture convergence mean that a smaller fraction of moisture diverges with increasing precipitation. Therefore, NMFC represents the strength of convection not only in the sense of the magnitude of vertical velocity but also in its effectiveness in converging moisture by virtue of its vertical profile. The relationship between the divergence profile and precipitation implies that NMFC increases with precipitation, and the relationship is approximately linear as demonstrated in Fig. 4b. Figure 4c shows the linear relationship derived by calculating the mean NMFC values within equally sized precipitation bins to find the intercept (0.13 mm h^{-1}) at which, in a mean sense, evaporation balances precipitation [Eq. (4)]. The value of pw at which this balance occurs, pw_0, which is an important parameter in the subsequent discussion, is also calculated in a similar manner (Fig. 4d). Defining the inverse of the slope of the regression line in Fig. 4c as the precipitable water limit pw_{lim} and the intercept as $E_0/\text{pw}_{\text{lim}}$,

$$\text{NMFC} = \frac{P - E_0}{\text{pw}_{\text{lim}}}. \tag{5}$$

Before moving the analysis further, a brief discussion of NMFC in the context of previous work is warranted. The normalization introduced in Eq. (3) is also relevant to the concept of gross moist stability (GMS) put forward by Neelin and Held (1987) and further developed by Raymond et al. (2009) and many others. The relationship between these two concepts is made more explicit in the appendix. As a measure of the depth of the moisture convergence field, NMFC is also related to temperature and saturation. For example, if the circulation is shallow, moisture can converge and diverge close to the surface with little saturation and precipitation as the near-surface temperature is warmer than the temperature at upper levels, but the circulation could also be deep enough to allow significant saturation and condensation.

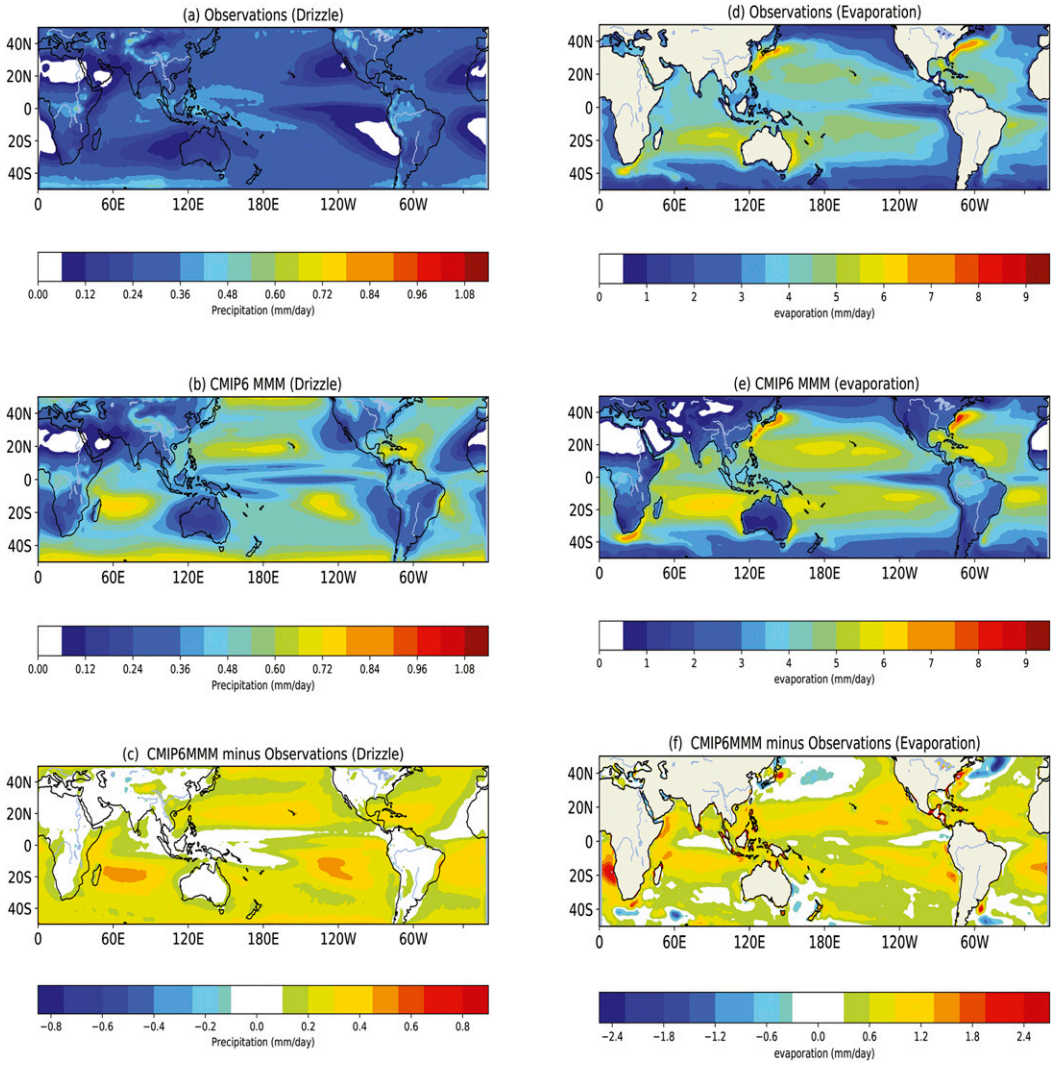

FIG. 2. (left) 15-yr (2000–14) mean drizzle precipitation (precipitation < 3.12 mm day^{-1}) from (a) TRMM-3B42 and PERSIANN (mm day^{-1}) and (b) multimodel mean of the 17 CMIP6 historical simulations, and (c) the difference of (b) minus (a). (right) 15-yr (2000–14) mean evaporation from (d) Woods Hole OA Flux Project evaporation (mm day^{-1}) and (e) multimodel mean of the 17 CMIP6 historical simulations, and (f) the difference of (e) minus (d).

Substituting Eq. (5) into Eq. (4), the moisture budget equation can be written as

$$\frac{\partial(\mathrm{pw})}{\partial t} \approx \left(E - \frac{\mathrm{pw}E_0}{\mathrm{pw}_{\mathrm{lim}}}\right) - P\left(1 - \frac{\mathrm{pw}}{\mathrm{pw}_{\mathrm{lim}}}\right). \tag{6}$$

To understand the physical meanings of $\mathrm{pw}_{\mathrm{lim}}$ and E_0, consider Eq. (6) as pw approaches $\mathrm{pw}_{\mathrm{lim}}$. In that case pw becomes less and less sensitive to precipitation. On the other hand, combining Eq. (3) and Eq. (5) yields the following:

$$-\frac{1}{g}\int_{\mathrm{pt}}^{\mathrm{ps}} \nabla \cdot (\mathbf{v}q)\, dp = (P - E_0)\left(\frac{\mathrm{pw}}{\mathrm{pw}_{\mathrm{lim}}}\right). \tag{7}$$

As pw approaches $\mathrm{pw}_{\mathrm{lim}}$, the loss of moisture by the net precipitation is compensated for by the gain through moisture convergence. Thus, $\mathrm{pw}_{\mathrm{lim}}$ represents an asymptotic limit for pw in the P–pw relationship at which precipitation is balanced by moisture convergence. On the other hand, E_0 represents the evaporation at grid points where there is drizzle but no moisture convergence. It is considered constant over the domain and the value is given for each model (legend in Fig. 6).

The above derivations and analyses show that the moisture budget can be used to understand the relative control of moisture convergence and evaporation on precipitation in the low-intensity and high-intensity regimes. Here we will demonstrate that the P–pw relationship can be derived from the moisture budget using the physical quantities $\mathrm{pw}_{\mathrm{lim}}$, pw_0, and E_0 defined above. Under steady state Eq. (6) can be written as

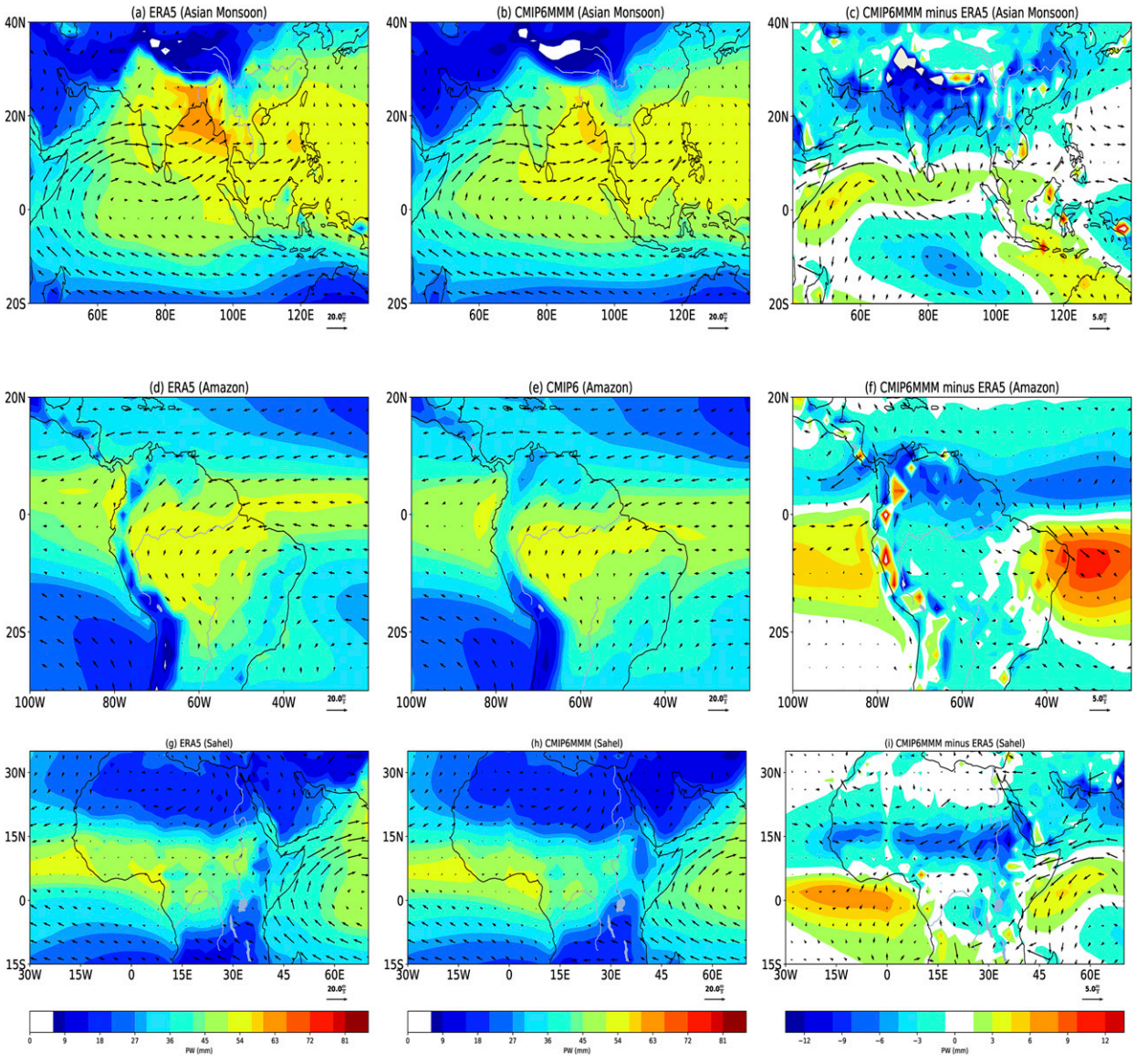

FIG. 3. Mean local summer precipitable water and 850-hPa circulation for three tropical landmasses from (a),(d),(g) ERA5 and (b),(e),(h) CMIP6 MMM, and (c),(f),(i) their differences.

$$P = \frac{E - \dfrac{\mathrm{pw}}{\mathrm{pw}_{\mathrm{lim}}} E_0}{1 - \dfrac{\mathrm{pw}}{\mathrm{pw}_{\mathrm{lim}}}}. \tag{8}$$

Equation (8) provides a P–pw relationship but it is not unique since it depends on evaporation. Of all the P–pw curves that arise from Eq. (8), the one that goes through ($\mathrm{pw} = \mathrm{pw}_0$, $E = E_0$) is of most interest to us as it represents the mean P–pw relationship when variability in evaporation and precipitable water tendencies are neglected. Therefore, the numerator in (8) becomes $E_0(1 - \mathrm{pw}_0/\mathrm{pw}_{\mathrm{lim}})$. After collecting ($\mathrm{pw}_{\mathrm{lim}} - \mathrm{pw}_0$) and ($\mathrm{pw} - \mathrm{pw}_0$) from the numerator and denominator respectively, Eq. (8) can be written as

$$P = \frac{E_0}{1 - \left(\dfrac{\mathrm{pw} - \mathrm{pw}_0}{\mathrm{pw}_{\mathrm{lim}} - \mathrm{pw}_0}\right)}. \tag{9}$$

It should be noted that (9) is not prognostic; rather, it should be interpreted as a state defined by precipitation drying, precipitable water, and the vertical structure of moisture convergence about which P and pw fluctuate under the prescribed evaporation E_0.

The analysis of Fig. 4 is repeated with all 17 CMIP6 historical simulations (Fig. 5) and the 10 SSP585 simulations (not shown), showing that the linear relationship in Fig. 4b based on ERA5 holds for the CMIP6 models. The model results are shown in blue, green, and red based on the value of $\mathrm{pw}_{\mathrm{lim}}$, the

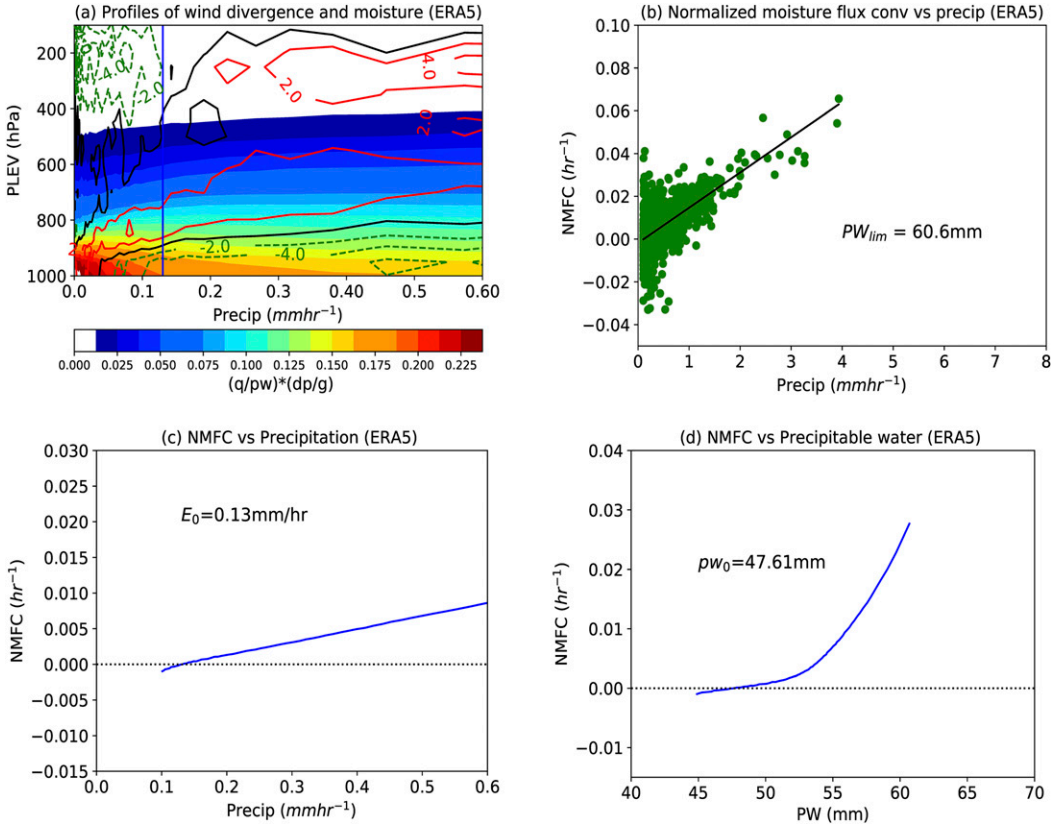

FIG. 4. (a) The relationship of water vapor profile (shading) and wind divergence ($10^5\ s^{-1}$) with precipitation in ERA5. The blue line represents the approximate precipitation value where the NMFC is zero. (b) Moisture flux convergence profile [NMFC; Eq. (3)] vs precipitation. The term pwlim is defined as the inverse of the slope of the regression line. (c) The relationship between precipitation and normalized moisture flux convergence (NMFC) for ERA5. (d) As in (c), but against precipitable water the points at which (NMFC) is zero. Values of E_0 and pw_0 are shown.

asymptotic pw limit, falling in the lower, middle, and higher terciles, respectively, of the multimodel ensemble. This color scheme is used in all subsequent plots. The parameter pw_{lim} varies widely among models. Similarly, the x-intercept value E_0 for which evaporation at NMFC equals zero [Eq. (5)] is shown in Fig. 6a for each CMIP6 historical simulation. Note that E_0 has a range of values between 0.15 to 0.19 mm h^{-1}, all higher than that for ERA5, which is 0.13mm h^{-1}. We set the threshold for drizzle precipitation as the value of E_0 derived from ERA5 (E_0 = 0.13 mm h^{-1} or 3.12 mm day^{-1}). Recall that E_0 corresponds to the evaporation (and precipitation) rate when NMFC is equal to zero. Rain rates below this E_0 threshold, defined as low-intensity precipitation, are primarily controlled by evaporation rather than by moisture convergence. Note that this threshold is smaller than 0.3 mm h^{-1} typically used as the drizzle threshold in an operational context (e.g., *AMS Glossary*).

Equation (9) implies that one can construct the relationship between P and pw from pw_{lim}, pw_0, and E_0, which are already obtained for each model from the above analysis. Figure 7a shows the actual relationship obtained by partitioning the 15 years of daily pw (tropical ocean points only) into 80 bins and averaging the corresponding daily precipitation in each bin. Figure 7b is the idealized relationship reconstructed from Eq. (9) using values of pw_{lim}, pw_0, and E_0 determined for each model. The idealized relationship captures the main features of the P–pw relationship and the differences among the models, as demonstrated by the correspondence between the color associated with each model relative to ERA5 in the two panels. Our analysis shows that, to first order, the relationship between precipitation and precipitable water 1) is governed by moisture conservation and 2) can be uniquely defined by two pw values pw_{lim} and pw_0. When pw approaches pw_{lim}, precipitation is balanced by moisture convergence, but when pw approaches pw_0 precipitation is balanced by evaporation. Each critical pw value is set by the vertical structure of moisture convergence and its relation to precipitation (Fig. 4). In many ways, pw_0 and pw_{lim} together play similar roles as w_c and β of Neelin et al. (2009) in that they determine the "pickup point" and the growth rate of precipitation with pw. As the atmosphere warms up, they both increase such that the P–pw curves shift and stretch to the right, as one would expect from the Clausius–Clapeyron relation. The idealized P–pw relationship will be used to analyze model diversity and biases from the CMIP6 simulations next.

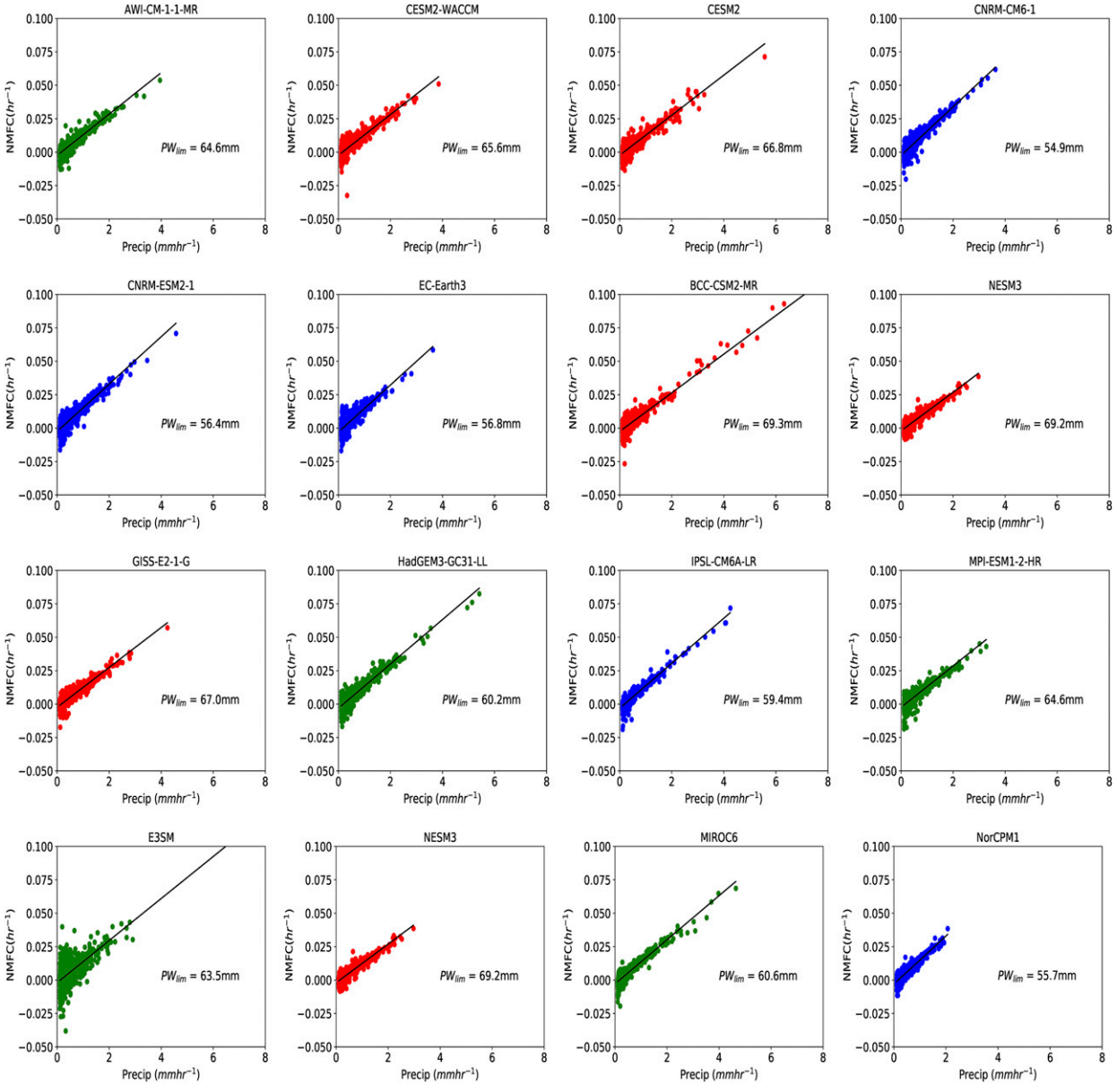

FIG. 5. As in Fig. 4b, but for 16 of the CMIP6 model historical simulations. The blue, green, and red colors correspond to models with low, medium, and high historical pw_{lim}, respectively.

b. *Normalization of precipitable water*

Here we examine the origins of precipitation biases and intermodel spread. Since the *P*–pw curves for the diverse models are of the same form, appropriate normalization could yield a general relationship for a straightforward interpretation.

Equation (9) can be written more concisely by defining a normalized precipitable water as $pw_n = pw/(pw_{lim} - pw_0)$, such that

$$P = \frac{E_0}{1 - (pw_n - pw_{nc})}, \tag{10}$$

where

$$pw_{nc} = \frac{pw_0}{pw_{lim} - pw_0} \tag{11}$$

is defined as the normalized critical precipitable water.

Equation (10) implies that precipitation can be estimated using $pw_n - pw_{nc}$ and E_0. The raw and normalized forms of the *P*–pw relationship are plotted in Figs. 8a and 8c, while the actual and estimated *P* frequency distributions are plotted in Figs. 8b and 8d. As predicted by Eq. (10) normalization reduces the spread in the *P*–pw relationships and in the pw frequency distributions. Note, however, that the normalized *P*–pw curves diverge near $pw_n - pw_{nc} = 0.5$ (Fig. 8c); because of the nonlinearity, small differences at higher PW lead to larger spread in precipitation than at low pw.

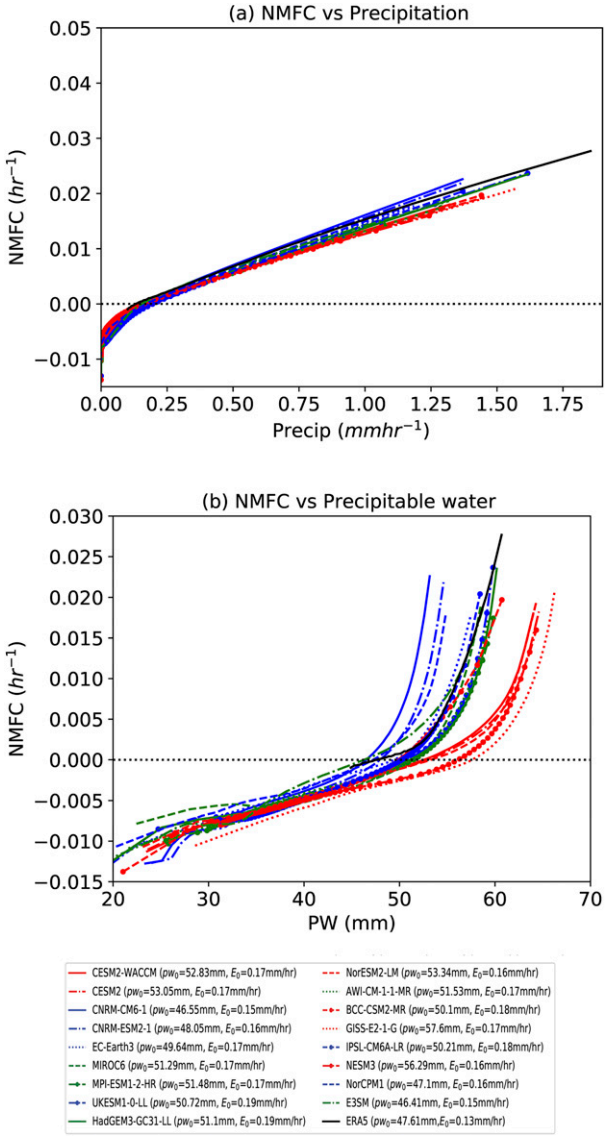

FIG. 6. (a) The relationship between precipitation and normalized moisture flux convergence (NMFC) for all the CMIP6 historical simulations. (b) As in (a), but against precipitable water. E_0 and pw_0 are provided in the legend. The blue, green, and red colors correspond to models with low, medium, and high historical pw_{lim}, respectively.

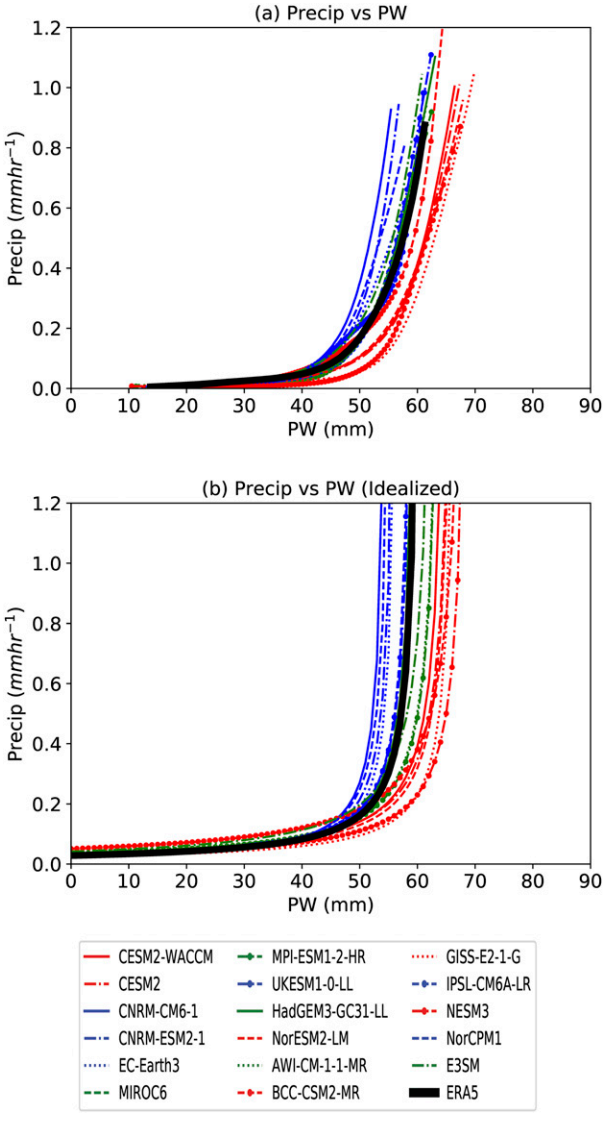

FIG. 7. (a) The relationship between precipitation and precipitable water from the models and ERA5, and (b) that derived from Eq. (9) using the respective E_0, pw_{lim}, and pw_0 values for each CMIP6 model historical simulation and for ERA5. The blue, green, and red colors correspond to models with low, medium, and high pw_{lim}, respectively.

To understand the physical implications of Eq. (10), consider the normalized P–pw relationship at its limits. At one extreme with $pw_n \ll pw_{nc}$, $P \approx E_0/(1 + pw_{nc})$. That is, precipitation is largely controlled by surface evaporation and is essentially independent of the local precipitable water. This regime corresponds to the widespread drizzle over high evaporation areas. In Fig. 4a, $pw_n \ll pw_{nc}$ corresponds to strong subsidence (left of the blue line) where wind divergence is confined to shallow levels, efficiently transporting moisture out of the column. At the other extreme with $pw_n \to 1 + pw_{nc}$ or $pw \to pw_{lim}$, P/E_0 becomes very large (Figs. 8a,c) and is much more sensitive to the precipitable water. Thus pw_{nc} can be thought of as a form of convective inhibition (e.g., the strength of upper-level convergence and subsidence in Fig. 4a) that a moist column must overcome to transition to deep convection. Before discussing the implications of this for model biases and projections the next section, there is one more point worth mentioning. Equation (10) is of the form $y = 1/(1 - x)$, which at first glance appears different from exponential form used in several previous studies to empirically fit observed and modeled P–pw relationships. Note however that for small x, $1/(1 - x)$ can be approximated by $1 + x$, which is also true for e^x. That

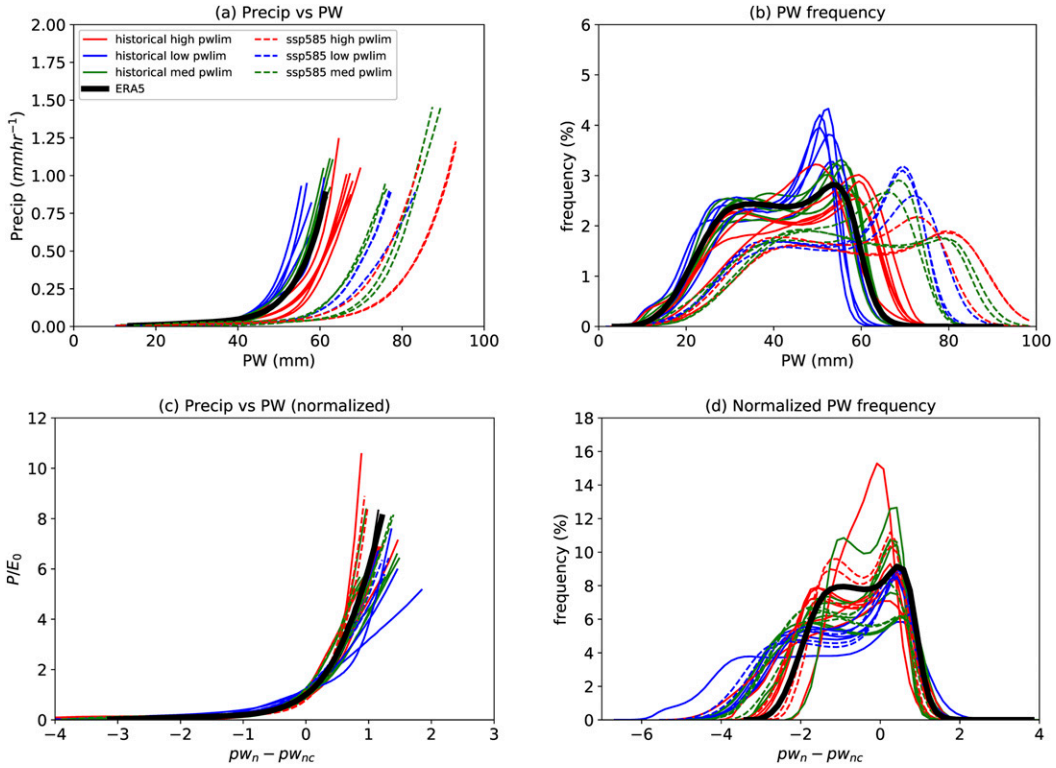

FIG. 8. (a) The relationship between precipitation and precipitable water in historical and ssp585 simulations and (b) the frequency distributions of precipitable water. (c),(d) As in (a) and (b), but both pw and P are normalized (see text). The blue, green, and red colors correspond to models with low, medium, and high historical pw_{lim}, respectively.

appears to us to be a mathematical coincidence. The above analysis suggests that the former is a physically sound relationship since it follows from conservation of moisture, mass, and energy under weak temperature gradient.

4. Model biases and projections

a. *Characterizing model biases and spread*

The convergence of the P–pw relationship (Fig. 8c) and the frequency distribution of pw after normalization (Fig. 8d) suggests that pw_{nc}, a measure of convective inhibition, and E_0, the evaporation under neutral NMFC (i.e., NMFC = 0), may be useful metrics for characterizing rainfall biases in models. Figure 9 shows a scatterplot of these two parameters. In comparison to the parameters derived from ERA5, all models have higher E_0, implying that the models produce more rain in the form of drizzle than ERA5 in the absence of moisture convergence (Figs. 2 and 6a). Most models also have higher pw_{nc} than ERA5, implying stronger convective inhibition than in observations, which means it takes more moisture to transition from drizzle to intense convection in the models. The fact that most models overestimate pw_{nc} implies they have a greater-than-observed frequency of days with pw_n smaller than pw_{nc} (or $pw < pw_0$; Fig. 8d). Most of the models have frequency distribution with respect to $pw_n - pw_{nc}$ that is extended to the left compared to ERA5 (Fig. 8d).

The difference in mean drizzle precipitation (daily precipitation $<$ 3.12 mm day^{-1}) between the five models with lowest and highest pw_{nc} is shown in Fig. 10. As predicted by the analysis, the low pw_{nc} models have much less drizzle. These models also simulate heavier total precipitation over Africa, South Asia, and the Maritime

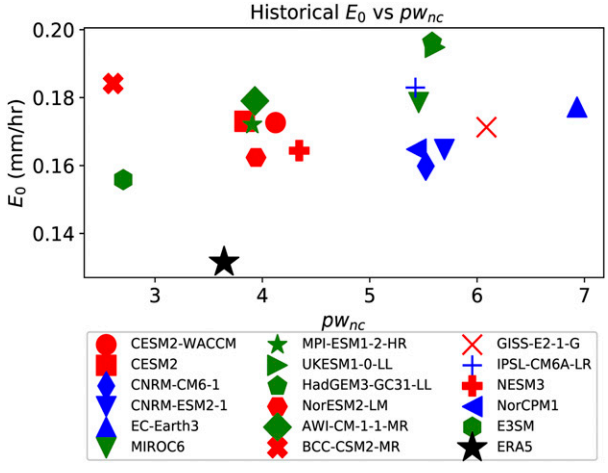

FIG. 9. (a) Scatterplot of E_0 vs pw_{nc} for the 17 CMIP6 models and ERA5 dataset.

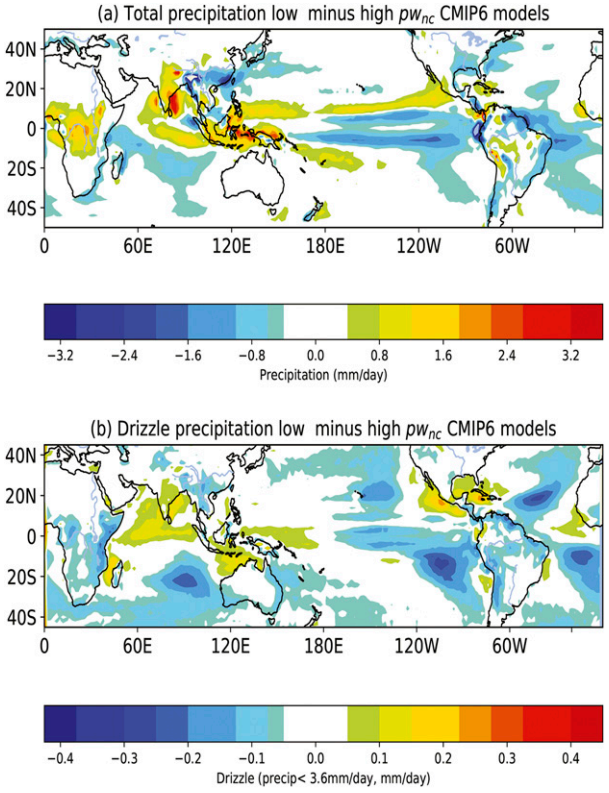

FIG. 10. (a) The difference in mean precipitation between the top and bottom five models according to their critical normalized precipitable water (pw_{nc}). (b) As in (a), but for precipitation $< 3.12\,\text{mm day}^{-1}$.

Continent. These results support the hypothesis put forward in the first section that the dry bias over tropical land may be related to the excess low-intensity precipitation over the high evaporation regions of the tropical ocean that limits the moisture transported to the landmasses through geostrophic adjustment.

b. *Projected change in precipitation*

Finally, the response to warming is examined in the normalized precipitable water framework. To understand the implication of the normalization of precipitation for projected change in precipitation, we consider the partial derivative of Eq. (9) with respect to E_0 and pw_{nc}:

$$\frac{\Delta P}{P} \approx \frac{\Delta E_0}{E_0} - \left[\frac{P}{E_0}\right] \Delta pw_{nc}. \tag{12}$$

Note that the term in the square brackets is nearly model independent and does not change much with warming as implied by the collapse of the P–pw curves into one after normalization (Fig. 8c). Figure 11 shows the end of the twenty-first-century fractional change in precipitation under the SSP585 scenario versus the corresponding change in pw_{nc} and E_0. The change in precipitation has a stronger relationship with Δpw_{nc} under warming than with ΔE_0. Six of the 10 models show a decrease in Δpw_{nc} and they have larger fractional increase in precipitation. As pw_{nc} is a function of pw_0 and pw_{lim} [Eq. (11)], its future change represents the combined effect of both thermodynamic change (increase in moisture represented here by increase in pw_{lim}) and the dynamic change (increase in inhibition or stability represented by increase in pw_0). Figure 11c shows the changes in both pw_{lim} and pw_0. Both changes are also depicted in the rightward shift of the P–pw curve and the pw frequency under warming (Figs. 8a,b, dashed lines). The dominance of thermodynamic change is reflected in the stronger response of pw_{lim} to warming (and therefore the decrease in pw_{nc}). Both changes in pw_{lim} and pw_0 in the models as responses to warming are related to the equilibrium climate sensitivity (ECS) of the models (Fig. 11d). Models with larger climate sensitivity have a larger change in pw_{lim} as one would expect from the Clausius–Clapeyron relation and a corresponding larger increase in pw_0 as stability increases as well.

c. *Historical trends*

In the last subsection we show that the change in precipitation in response to warming can be represented by the decrease in pw_{nc}, that is, the net decrease in convective inhibition resulting from the competing effects of increase in moisture (pw_{lim}) and increase in pw_0 (Fig. 11c). This raises the question of whether trends in pw_{lim} and pw_0 can be detected in the global reanalysis and the observed precipitation. To address this question the trends in 40 years of pw_{lim} and pw_0 values are calculated from ERA5. Because of the nonlinear nature of the P–pw relationship, a slight decrease in pw_{nc} leads to a shift of many points from the evaporation-controlled drizzle regime to the pw-controlled regime. Thus we expect a rapid increase in precipitation near pw_{nc}. To verify this expectation, we computed the historical precipitation trends using 36 years of PERSIANN daily drizzle precipitation (precipitation $< 3.12\,\text{mm day}^{-1}$ as defined above). Figure 12 shows the trends normalized by their corresponding historical mean values. The statistical significances of the trend in ERA5 pw_{lim} and pw_0 as well as that of the drizzle precipitation trend from PERSIANN are tested using the Kendall's tau (KT) test (Kornbrot 2014) and the p values shown in the figure indicate that the trends are statistically significant. Even though there are also increasing trends in the critical normalized precipitable water from ERA5 and total precipitation from PERSIANN (not shown), they are not found to be statistically significant according to the KT test. This is consistent with the competing effects of the changes in pw_{lim} versus pw_0 on the changes in pw_{nc}, rendering larger uncertainty in estimating the changes in pw_{nc} and the total precipitation compared to the changes in drizzle precipitation, which are determined by changes in pw_0 alone.

5. Conclusions

Several previous studies have documented the excess precipitation over tropical oceans and dry biases over tropical landmasses in multiple generations of CMIP models. Motivated by these persistent biases and the uncertainties in the projected changes, we developed a new framework to study the moisture budgets of the ERA5 dataset and CMIP6 simulations. This framework reveals that the regional distribution of precipitation, specifically whether precipitation occurs preferentially over high

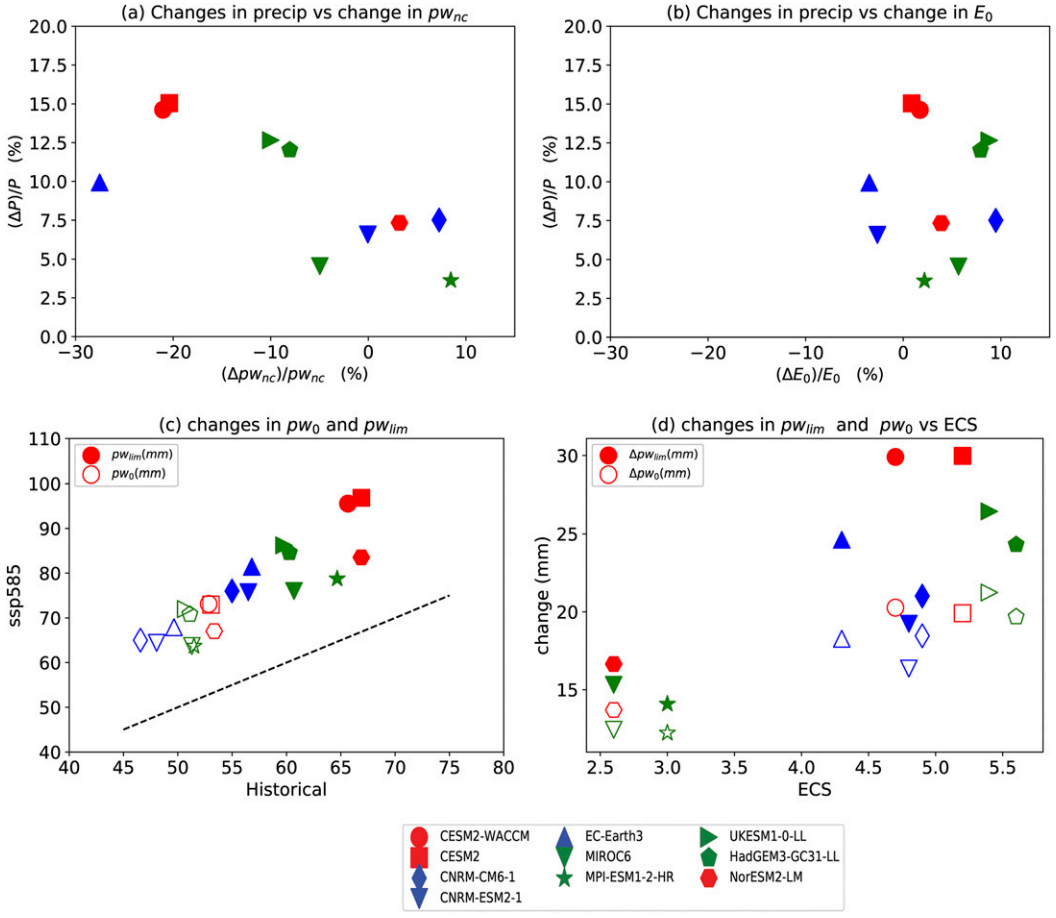

FIG. 11. (a) The percentage difference in P vs in pw_{nc} between historical (2000–14) and SSP585 (2086–2100) simulations. (b) As in (a), but for change in P and in E_0. (c) SSP585 pw_0 and pw_{lim} (mm) vs their historical values. (d) Change in pw_0 and pw_{lim} (mm) under the SSP585 scenario vs equilibrium climate sensitivity (ECS).

evaporation areas (which leads to "double ITCZ") or high precipitable water areas (Fig. 10), is related to the vertical structure of moisture flux convergence and how it relates to precipitation intensity. It is shown that the well-documented relationship between precipitation (P) and column integrated precipitable water (pw) can be uniquely defined by two critical pw values: the pw where precipitation balances evaporation, and the pw where precipitation balances moisture flux convergence (Fig. 6). When the raw pw is scaled by the difference of these two values, one can define a normalized critical precipitable water, pw_{nc}, which is a measure of convective inhibition that separates tropical precipitation into two regimes: a local evaporation-controlled regime with widespread drizzle, and a precipitable water–controlled regime with heavy rainfall. Compared to ERA5, most of the 17 CMIP6 model historical simulations examined have both higher pw_{nc} (convective inhibition) and E_0 (evaporation and precipitation balance point), and too much drizzle (Fig. 9). It is also shown that the magnitude of the response to warming is also linearly related to the change in pw_{nc}. A robust increasing trend in both the pw values that define the P–pw relationship are detected in ERA5 and the implied trend of low-intensity precipitation is also observed in the PERSIANN precipitation dataset (Fig. 12).

There is increased recognition of the role of representation of entrainment and detrainment processes in defining the P–pw relationship, not just in the inhibition or promotion of convection by environmental moisture at diurnal and subdiurnal time scales (Derbyshire et al. 2004; Tompkins 2001; Ahmed and Neelin 2018) but also through the impact of convection on the moisture budget of the column itself at longer time scales (Kuo et al. 2017; Singh et al. 2019; Emanuel 2019). In the framework presented in this study, we use daily averages of P and pw, and the analytical solutions are derived from a steady-state form of conservation of moisture; thus, they represent a steady-state relationship about which P and pw fluctuate. From the short time scale perspective, the critical normalized precipitable water derived in this study represents a measure of inhibition that the normalized moisture must exceed for deep convection to take place. That inhibition depends on the how rapidly the updraft deepens with increasing precipitation and therefore to what extent the column-integrated moisture convergence compensates for the moisture loss by precipitation. Thus, the normalized precipitable water framework (specifically the critical normalized precipitable water parameter) could be a theoretical tool for interpreting the combined

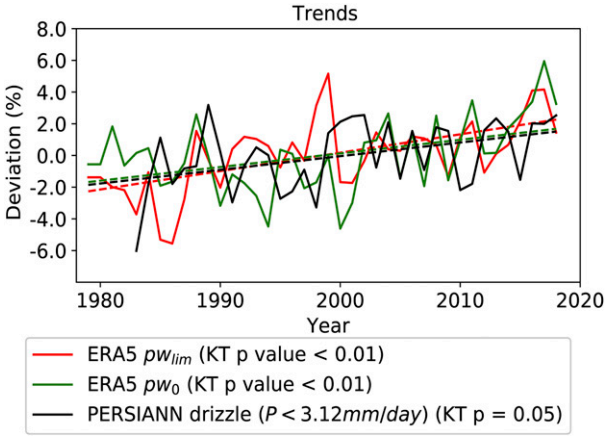

FIG. 12. (a) The trends in pw_{lim} and pw_0 from ERA5 data as well as in the amount of drizzle precipitation (precipitation rate < 3.12 mm day^{-1}; see text) averaged over the tropical oceans. All three trends are plotted as deviations from their respective long-term means and pass the Kendall's tau statistical significance test at the level indicated in the legend.

effects of promotion of convection by environmental moisture as well as the moistening effect of convection in parameterizations of entrainment and detrainment in climate models. Furthermore, although the normalized precipitable water framework is inherently nonspatial, it can provide insights into model biases in the spatial distribution of rainfall, particularly over tropical landmasses versus ocean.

Acknowledgments. This is work is supported by U.S. Department of Energy Office of Science Biological and Environmental Research as part of Global and Regional Modeling and Analysis Program. The contribution of YG is supported by National Oceanic and Atmospheric Administration (NOAA) Oceanic and Atmospheric Research, Program Climate Program Office (CPO), under NOAA Grant NA17OAR4310263. Computing resources for the analysis are provided by the National Energy Research Scientific Computing Center (NERSC). We acknowledge the World Climate Research Programme, which, through its Working Group on Coupled Modelling, coordinated and promoted CMIP6. We thank the climate modeling groups for producing and making available their model output, the Earth System Grid Federation (ESGF) for archiving the data and providing access, and the multiple funding agencies who support CMIP6 and ESGF. We thank DOE's RGMA program area, the Data Management program, and NERSC for making this coordinated CMIP6 analysis activity possible. Pacific Northwest National Laboratory is operated by Battelle for the U.S. Department of Energy under Contract DE-AC05-76RLO1830. The global ocean heat flux and evaporation products were provided by the WHOI OAFlux project (http://oaflux.whoi.edu) funded by the NOAA Climate Observations and Monitoring (COM) program. We also would like to thank Daehyun Kim for insightful feedback on the early versions of the manuscript.

APPENDIX

Relationship between Normalized Moisture Flux Convergence and Gross Moist Stability

Using the steady-state form of the dry static energy and moisture equations [Eq. (2.3) in Raymond et al. 2009], normalized gross moist stability can be written as

$$\Gamma_R = -\frac{T_R \int_{pt}^{ps} \nabla \cdot (vs)\, dp}{L \int_{pt}^{ps} \nabla \cdot (vq)\, dp}, \tag{A1}$$

where $T_R = 300$ K is a reference temperature, L is the latent heat of condensation, v is horizontal wind, and s is specific moist entropy. Combined with Eq. (3), (A1) can be rewritten as

$$\mathrm{NMFC} = -\frac{T_R \int_{pt}^{ps} \nabla \cdot (vs)\, dp}{\mathrm{Lpw}\Gamma_R}. \tag{A2}$$

Using Eq. (2.1) of Raymond et al. (2009), again for steady state, (A2) can be written as

$$-\Gamma_R \mathrm{NMFC} = \frac{T_R(F_s - R)}{\mathrm{Lpw}}, \tag{A3}$$

where F_s is the moist entropy flux due to surface fluxes of heat and moisture and R is the pressure integral of the entropy sink due to radiative cooling. Equation (A3) states that the strength of convection (NMFC) is related to the diabatic heating and stability. This is analogous to the weak temperature gradient representation of the energy conservation (Holton 1992):

$$-S_p \omega = J/C_p, \tag{A4}$$

where S_p is static stability, ω is pressure vertical velocity, and J is diabatic heating. Hence it is not surprising that the linear relationship between NMFC with precipitation follows from (A4) (Hagos et al. 2019).

REFERENCES

Ahmed, F., and C. Schumacher, 2015: Convective and stratiform components of the moisture–precipitation relationship. *Geophys. Res. Lett.*, **42**, 10 453–10 462, https://doi.org/10.1002/2015GL066957.

——, and J. D. Neelin, 2018: Reverse engineering the tropical precipitation–buoyancy relationship. *J. Atmos. Sci.*, **75**, 1587–1608, https://doi.org/10.1175/JAS-D-17-0333.1.

Allen, M., and W. J. Ingram, 2002: Constraints on future changes in climate and the hydrologic cycle. *Nature*, **419**, 228–232, https://doi.org/10.1038/nature01092.

Ashouri, H., K.-L. Hsu, S. Sorooshian, D. K. Braithwaite, K. R. Knapp, L. D. Cecil, B. R. Nelson, and O. P. Prat, 2015: PERSIANN-CDR: Daily precipitation climate data record from multisatellite observations for hydrological and climate studies. *Bull. Amer. Meteor. Soc.*, **96**, 69–83, https://doi.org/10.1175/BAMS-D-13-00068.1.

Bretherton, C. S., M. E. Peters, and L. E. Back, 2004: Relationships between water vapor path and precipitation over the tropical oceans. *J. Climate*, **17**, 1517–1528, https://doi.org/10.1175/1520-0442(2004)017<1517:RBWVPA>2.0.CO;2.

Chikira, M., 2010: A cumulus parameterization with state-dependent entrainment rate. Part II: Impact on climatology in a general circulation model. *J. Atmos. Sci.*, **67**, 2194–2211, https://doi.org/10.1175/2010JAS3317.1.

Dai, A., 2006: Precipitation characteristics in eighteen coupled climate models. *J. Climate*, **19**, 4605–4630, https://doi.org/10.1175/JCLI3884.1.

Demory, M. E., P. L. Vidale, M. J. Roberts, P. Berrisford, J. Strachan, R. Schiemann, and M. S. Mizielinski, 2014: The role of horizontal resolution in simulating drivers of the global hydrological cycle. *Climate Dyn.*, **42**, 2201–2225, https://doi.org/10.1007/s00382-013-1924-4.

Derbyshire, S. H., I. Beau, P. Bechtold, J.-Y. Grandpeix, J.-M. Piriou, J.-L. Redelsperger, and P. M. M. Soares, 2004: Sensitivity of moist convection to environmental humidity. *Quart. J. Roy. Meteor. Soc.*, **130**, 3055–3079, https://doi.org/10.1256/qj.03.130.

Emanuel, K., 2019: Inferences from simple models of slow, convectively coupled processes. *J. Atmos. Sci.*, **76**, 195–208, https://doi.org/10.1175/JAS-D-18-0090.1.

Emori, S., T. Nozawa, A. Numaguti, and I. Uno, 2001: Importance of cumulus parameterization for precipitation simulation over East Asia in June. *J. Meteor. Soc. Japan*, **79**, 939–947, https://doi.org/10.2151/jmsj.79.939.

Fiedler, S., and Coauthors, 2020: Simulated tropical precipitation assessed across three major phases of the Coupled Model Intercomparison Project (CMIP). *Mon. Wea. Rev.*, **148**, 3653–3680, https://doi.org/10.1175/MWR-D-19-0404.1.

Hagos, S., L. R. Leung, M. Ashfaq, and K. Balaguru, 2019: South Asian monsoon precipitation in CMIP5: A link between inter-model spread and the representations of tropical convection. *Climate Dyn.*, **52**, 1049–1061, https://doi.org/10.1007/s00382-018-4177-4.

Held, I. M., and B. J. Soden, 2006: Robust responses of the hydrologic cycle to global warming. *J. Climate*, **19**, 5686–5699, https://doi.org/10.1175/JCLI3990.1.

Hirota, N., and Y. N. Takayabu, 2013: Reproducibility of precipitation distribution over the tropical oceans in CMIP5 multi-climate models compared to CMIP3. *Climate Dyn.*, **41**, 2909–2920, https://doi.org/10.1007/s00382-013-1839-0.

——, ——, M. Watanabe, and M. Kimoto, 2011: Precipitation reproducibility over tropical oceans and its relationship to the double ITCZ problem in CMIP3 and MIROC5 climate models. *J. Climate*, **24**, 4859–4873, https://doi.org/10.1175/2011JCLI4156.1.

Holloway, C. E., and J. D. Neelin, 2009: Moisture vertical structure, column water vapor, and tropical deep convection. *J. Atmos. Sci.*, **66**, 1665–1683, https://doi.org/10.1175/2008JAS2806.1.

Holton, J. R., 1992: *An Introduction to Dynamic Meteorology*. 3rd ed., Academic Press, 511 pp.

Huffman, G. J., R. F. Adler, D. T. Bolvin, and E. J. Nelkin, 2010: The TRMM Multi-Satellite Precipitation Analysis (TMPA). *Satellite Rainfall Applications for Surface Hydrology*, F. Hossain and M. Gebremichael, Eds., Springer Verlag, 3–22.

Igel, M. R., S. R. Herbener, and S. M. Saleeby, 2017: The tropical precipitation pickup threshold and clouds in a radiative convective equilibrium model: 1. Column moisture. *J. Geophys. Res. Atmos.*, **122**, 6453–6468, https://doi.org/10.1002/2016JD025907.

Kornbrot, D., 2014: Kendall's tau: Basic. *Wiley StatsRef: Statistics Reference Online*, N. Balakrishnan et al., Eds., https://doi.org/10.1002/9781118445112.stat06566.

Kuo, Y.-H., J. D. Neelin, and C. R. Mechoso, 2017: Tropical convective transition statistics and causality in the water vapor–precipitation relation. *J. Atmos. Sci.*, **74**, 915–931, https://doi.org/10.1175/JAS-D-16-0182.1.

Liu, Z., A. Mehran, T. J. Phillips, and A. AghaKouchak, 2014: Seasonal and regional biases in CMIP5 precipitation simulations. *Climate Res.*, **60**, 35–50, https://doi.org/10.3354/cr01221.

Neelin, J. D., and I. M. Held, 1987: Modeling tropical convergence based on the moist static energy budget. *Mon. Wea. Rev.*, **115**, 3–12, https://doi.org/10.1175/1520-0493(1987)115<0003:MTCBOT>2.0.CO;2.

——, O. Peters, and K. Hales, 2009: The transition to strong convection. *J. Atmos. Sci.*, **66**, 2367–2384, https://doi.org/10.1175/2009JAS2962.1.

Pendergrass, A. G., and D. L. Hartmann, 2014: The atmospheric energy constraint on global-mean precipitation change. *J. Climate*, **27**, 757–768, https://doi.org/10.1175/JCLI-D-13-00163.1.

Peters, O., J. D. Neelin, and S. W. Nesbitt, 2009: Mesoscale convective systems and critical clusters. *J. Atmos. Sci.*, **66**, 2913–2924, https://doi.org/10.1175/2008JAS2761.1.

Raymond, D. J., S. L. Sessions, A. H. Sobel, and Z. Fuchs, 2009: The mechanics of gross moist stability. *J. Adv. Model. Earth Syst.*, **1**, 9, https://doi.org/10.3894/JAMES.2009.1.9.

Rushley, S. S., D. Kim, C. S. Bretherton, and M.-S. Ahn, 2018: Reexamining the nonlinear moisture–precipitation relationship over the tropical oceans. *Geophys. Res. Lett.*, **45**, 1133–1140, https://doi.org/10.1002/2017GL076296.

Sahany, S., J. D. Neelin, K. Hales, and R. B. Neale, 2014: Deep convective transition characteristics in the Community Climate System Model and changes under global warming. *J. Climate*, **27**, 9214–9232, https://doi.org/10.1175/JCLI-D-13-00747.1.

Sillmann, J., V. V. Kharin, X. Zhang, F. W. Zwiers, and D. Bronaugh, 2013: Climate extremes indices in the CMIP5 multimodel ensemble: Part I. Model evaluation in the present climate. *J. Geophys. Res. Atmos.*, **118**, 1716–1733, https://doi.org/10.1002/jgrd.50203.

Singh, M. S., R. A. Warren, and C. Jakob, 2019: A steady-state model for the relationship between humidity, instability, and precipitation in the tropics. *J. Adv. Model. Earth Syst.*, **11**, 3973–3994, https://doi.org/10.1029/2019MS001686.

Small, R. J., F. O. Bryan, S. P. Bishop, and R. A. Tomas, 2019: Air–sea turbulent heat fluxes in climate models and observational analyses: What drives their variability? *J. Climate*, **32**, 2397–2421, https://doi.org/10.1175/JCLI-D-18-0576.1.

Sobel, A. H., and C. S. Bretherton, 2000: Modeling tropical precipitation in a single column. *J. Climate*, **13**, 4378–4392, https://doi.org/10.1175/1520-0442(2000)013<4378:MTPIAS>2.0.CO;2.

——, J. Nilsson, and L. M. Polvani, 2001: The weak temperature gradient approximation and balanced tropical moisture waves. *J. Atmos. Sci.*, **58**, 3650–3665, https://doi.org/10.1175/1520-0469(2001)058<3650:TWTGAA>2.0.CO;2.

Song, X., and G. Zhang, 2009: Convection parameterization, tropical Pacific double ITCZ, and upper-ocean biases in the NCAR CCSM3. Part I: Climatology and atmospheric feedback. *J. Climate*, **22**, 4299–4315, https://doi.org/10.1175/2009JCLI2642.1.

Sperber, K. R., H. Annamalai, I.-S. Kang, A. Kitoh, A. Moise, A. Turner, B. Wang, and T. Zhou, 2013: The Asian summer monsoon: An intercomparison of CMIP5 vs. CMIP3 simulations of the late 20th century. *Climate Dyn.*, **41**, 2711–2744, https://doi.org/10.1007/s00382-012-1607-6.

Stephens, G. L., and Coauthors, 2010: Dreary state of precipitation in global models. *J. Geophys. Res.*, **115**, D24211, https://doi.org/10.1029/2010JD014532.

Tompkins, A. M., 2001: Organization of tropical convection in low vertical wind shears: The role of water vapor. *J. Atmos. Sci.*, **58**, 529–545, https://doi.org/10.1175/1520-0469(2001)058<0529:OOTCIL>2.0.CO;2.

Yin, L., R. Fu, E. Shevliakova, and R. E. Dickinson, 2013: How well can CMIP5 simulate precipitation and its controlling processes over tropical South America? *Climate Dyn.*, **41**, 3127–3143, https://doi.org/10.1007/s00382-012-1582-y.

Yu, L., X. Jin, and R. A. Weller, 2008: Multidecade Global Flux Datasets from the Objectively Analyzed Air-sea Fluxes (OAFlux) Project: Latent and sensible heat fluxes, ocean evaporation, and related surface meteorological variables. Woods Hole Oceanographic Institution, OAFlux Project Tech. Rep. OA-2008-01, 64 pp..

Zhang, X., W. Lin, and M. Zhang, 2007: Toward understanding the double Intertropical Convergence Zone pathology in coupled ocean–atmosphere general circulation models. *J. Geophys. Res.*, **112**, D12102, https://doi.org/10.1029/2006JD007878.